Emergent interaction-induced topology in Bose-Hubbard ladders

David Wellnitz [1,2,*] Gustavo A. Domínguez-Castro,[3] Thomas Bilitewski,[4] Monika Aidelsburger,[5,6,7]
Ana Maria Rey [1,2] and Luis Santos [3,†]

[1]*JILA, National Institute of Standards and Technology and Department of Physics, University of Colorado, Boulder, Colorado 80309, USA*
[2]*Center for Theory of Quantum Matter, University of Colorado, Boulder, Colorado 80309, USA*
[3]*Institut für Theoretische Physik, Leibniz Universität Hannover, Appelstrasse 2, D-30167 Hannover, Germany*
[4]*Department of Physics, Oklahoma State University, Stillwater, Oklahoma 74078, USA*
[5]*Max-Planck-Institut für Quantenoptik, Hans-Kopfermann-Strasse 1, 85748 Garching, Germany*
[6]*Fakultät für Physik, Ludwig-Maximilians-Universität, Schellingstrasse 4, 80799 München, Germany*
[7]*Munich Center for Quantum Science and Technology (MCQST), Schellingstraße 4, 80799 München, Germany*

We investigate the quantum many-body dynamics of bosonic atoms hopping in a two-leg ladder with strong on-site contact interactions. We observe that when the atoms are prepared in a staggered pattern with pairs of atoms on every other rung, singlon defects, i.e., rungs with only one atom, can localize due to an emergent topological model, even though the underlying model in the absence of interactions admits only topologically trivial states. This emergent topological localization results from the formation of a zero-energy edge mode in an effective lattice formed by two adjacent chains with alternating strong and weak hoping links (Su-Schrieffer-Heeger chains) and opposite staggering which interface at the defect position. Our findings open the opportunity to dynamically generate nontrivial topological behaviors without the need for complex Hamiltonian engineering.

Topological phases of matter [1,2], including the quantum Hall effect [3–5] and topological insulators [6,7] have attracted significant attention for quantum science and technologies [8–11] given their robustness against disorder and defects. While noninteracting topological phases have been realized in a broad range of settings, both classical [12–15] and quantum [16–25], and are to a great extent well understood [26,27], interaction-enabled topological states remain largely unexplored. Understanding how topological phases may arise in interacting systems is hence an exciting, but challenging problem.

Ultracold gases [28–31] with tunable interactions in optical lattices and tweezer arrays [32] are emerging as an excellent platform to shed light on this direction [25,33,34], in particular with their capability to observe many-body states with single-site and spin resolution [35–42]. These have allowed the realization of noninteracting topological phases and observation of key underlying features [17–23], such as edge states and currents [17–19,43], Chern numbers [21], and topological pumping [22,23]. Progress towards the implementation of interacting systems such as many-body symmetry protected topological phases [2] include bosonic Su-Schrieffer-Heeger

(SSH) models [44] in interacting Rydberg atoms [45], fractional quantum Hall states with few atoms [46,47], and the Haldane phase in Fermi-Hubbard ladders [48,49]. However, especially for mobile particles, reaching the ultracold temperature necessary to observe interacting topological ground states remains a significant obstacle. While internal degrees of freedom can be pumped into a single state with essentially zero entropy, similar techniques do not exist for motion in lattices. It would be hence highly appealing to find settings where topology emerges naturally in the dynamics of a strongly interacting system [28–31,50,51] from an easy to prepare initial state.

In this Letter, we report on emerging interaction-induced topological localization in an experimentally accessible system of strongly interacting bosons in two-leg ladders. Two-leg ladders have played a major role as model systems for quantum magnetism [52,53], in nonequilibrium many-body dynamics, hydrodynamics and transport [54–60], and in realizations of synthetic magnetism [17]. More recently, bosons in optical ladders have been used to study nonequilibrium dynamics in the hard-core limit where strong interactions prevent more than one atom per site (a model equivalent to an XX spin ladder [55]). By initially preparing a density wave (DW) along the legs with filled (empty) sites in even (odd) rungs [Fig. 1(a)], experiments have observed within their accessible timescales a crossover from ballistic to diffusive correlation dynamics when the rung hopping ($J_\perp$) increases from zero to equal to the leg hopping ($J_\parallel$) [61].

Here we analyze the opposite regime when $\eta \equiv J_\perp/J_\parallel \gg 1$, focusing on experimentally accessible timescales. Besides radically different correlations in the hard-core limit, we find

*Contact author: david.wellnitz@colorado.edu
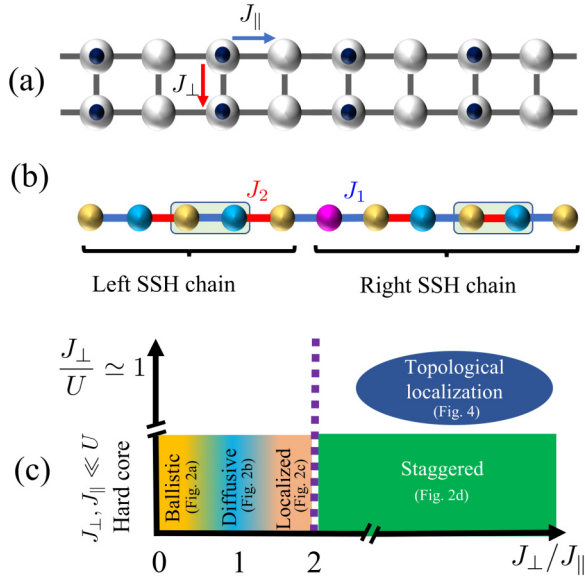†Contact author: santos@itp.uni-hannover.de

FIG. 1. (a) Bose-Hubbard ladder with rung (leg) hopping $J_\perp$ ($J_\parallel$). Initially there is one (no) particle per site in even (odd) rungs. (b) Emergent SSH chains of opposite staggering interface at a central site (purple), and emergent model in the dynamics of singlon defects. (c) Overview of the regimes. In the hard-core regime, $J_\perp, J_\parallel \ll U$, rung density-density (RDD) correlations are negative, and their expansion within relevant timescales transitions from ballistic to diffusive to localized when $\eta \equiv J_\perp/J_\parallel$ grows from 0 to 2. For $\eta > 2$, staggered RDD correlations expand ballistically. For $J_\parallel \ll J_\perp \lesssim U$, singlon defects experience topological or nontopological localization. We indicate which figures illustrate the regimes.

that, surprisingly, when the on-site interactions are large but finite, an initial isolated singlon defect in the DW pattern, i.e., a singly-occupied rung, experiences an emergent effective lattice composed of two SSH chains of opposite staggering, and hence different topology, that meet at the initial defect position [Fig. 1(b)]. These interfaces can feature two distinct types of localized states resulting in the localization of defects: (i) zero energy edge modes related to the SSH topology, and (ii) energetically bound states at the ends of the energy spectrum. Our analysis hence unveils a surprising link between topology and many-body dynamics in strongly interacting ladders. Contrary to other realizations of topological models in optical lattices [45,49,62], or topological interfaces of SSH chains in other systems [63–66], the SSH chain and the topological interface are not externally implemented, but emerge naturally from the interplay of interactions, motion and the original DW pattern. This intriguing physics [Fig. 1(c)] can be probed in on-going experiments.

Model. We consider bosons in a square ladder, see Fig. 1(a), with legs 1 and 2, described in the tight-binding regime by the Bose-Hubbard (BH) Hamiltonian $\hat{H} = \hat{H}_0 + \frac{U}{2}\sum_{i,\alpha} \hat{n}_{i,\alpha}(\hat{n}_{i,\alpha} - 1)$, with

$$\hat{H}_0 = -\sum_i \left(\frac{J_\parallel}{2}\sum_{\alpha=1,2} \hat{b}^\dagger_{i+1,\alpha}\hat{b}_{i,\alpha} + \frac{J_\perp}{2}\hat{b}^\dagger_{i,1}\hat{b}_{i,2} + \text{H.c.} \right), \quad (1)$$

where $\hat{b}_{i,\alpha}$ is the bosonic operator at site i of leg α, $\hat{n}_{i,\alpha} = \hat{b}^\dagger_{i,\alpha}\hat{b}_{i,\alpha}$, and U characterizes the on-site interactions.
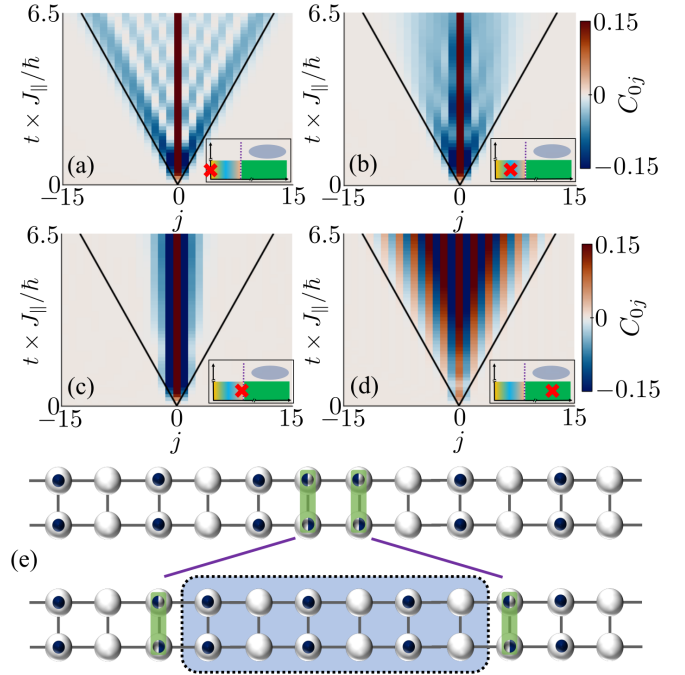

FIG. 2. Time evolution of the RDD correlation C_{0j} with $\eta = 0$ (a), 1 (b), 2 (c), and 8 (d). Simulations of the hard-core Hamiltonian $\hat{H}_0$ on 31 sites, using MPS with bond dimensions $\chi = 1536$ [(a) and (b)], 1024 (c), and 512 (d). The black lines correspond to the ballistic propagation when $\eta = 0$. The red "x" in the insets locates the plots in Fig. 1(c). (e) Mechanism leading to the staggered correlations in (d). Quantum fluctuations result in pairs of singlon defects (green), which when moving apart form a string of rungs (blue shaded area) with an inverted DW compared to the initial one.

Motivated by recent experiments [61] we assume large U, and consider an initial DW, in which sites at even (odd) rungs are occupied by one (no) atom.

Hard-core regime. To develop an intuition of the dynamical regimes, we first consider an idealized scenario without initial defects in the DW. Furthermore, we restrict the dynamics to the hard-core manifold described solely by $\hat{H}_0$ for very large $U \gg J_\perp, J_\parallel$. A Bogoliubov stability analysis shows that the DW is stable against the exponential proliferation of singlon defects if $\eta > 2$ (see [67] and also Ref. [56]). Indeed, $\eta \simeq 2$ marks the onset of clearly different dynamics. As in recent experiments [61], we consider rung density-density (RDD) correlations $C_{ij} = \langle \hat{n}_i \hat{n}_j \rangle - \langle \hat{n}_i \rangle \langle \hat{n}_j \rangle$, with $\hat{n}_i = \hat{n}_{i,1} + \hat{n}_{i,2}$ the particle number operator of rung i. Our results of $C_{0j}(t)$, obtained using Matrix Product State (MPS) calculations, show a markedly different behavior for $\eta < 2$ than for $\eta > 2$. For $\eta = 0$ [Fig. 2(a)], the system is integrable, and the correlations expand ballistically as $C_{0j}(t) = -\frac{1}{4}\mathcal{J}_j^2(2J_\parallel t/\hbar)$, with $\mathcal{J}_j$ the Bessel function of first kind. As discussed in Ref. [61], when η increases from 0 to 1 the expansion changes from ballistic to diffusive within the timescale of the experiments [Fig. 2(b)]. A further increase of η results in a strong slowdown of the evolution of the correlations, which within experimentally accessible timescales becomes clearly subdiffusive, and eventually approximately localized at $\eta = 2$ [Fig. 2(c)]. One would naively expect that the larger η the more localized C_{0j} would be. Interestingly, the nature of the correlations changes

remarkably at $\eta \simeq 2$. Whereas $C_{0j} < 0$ for $\eta < 2$, for $\eta > 2$ RDD correlations are staggered, $(-1)^j C_{0j} > 0$, and expand ballistically as for $\eta = 0$ [Fig. 2(d)].

To understand these dynamics for $\eta \gg 1$, we introduce the hard-core rung states: $|2\rangle \equiv (\begin{smallmatrix}\bullet\\\bullet\end{smallmatrix})$, $|0\rangle \equiv (\begin{smallmatrix}\circ\\\circ\end{smallmatrix})$, and $|\pm\rangle \equiv \frac{1}{\sqrt{2}}[(\begin{smallmatrix}\bullet\\\circ\end{smallmatrix}) \pm (\begin{smallmatrix}\circ\\\bullet\end{smallmatrix})]$, where $\bullet$ ($\circ$) denotes an occupied (empty) site. Quantum fluctuations due to leg hopping create singlon-defect pairs [Fig. 2(e)]: $|2, 0\rangle \to |+, +\rangle - |-, -\rangle$, with a density $1/\eta^2$. These defects, initially at neighboring sites, drift apart with rate $J_\parallel$ by position swaps between $|\pm\rangle$ and $|2\rangle$ or $|0\rangle$ induced by the leg hopping [Fig. 2(e)]. After a time t, the defects have a probability $\mathcal{J}_{r-1}^2(2J_\parallel t)$ to be at $r \geq 1$ sites apart [67]. The rungs in between the defects present an inverted DW pattern compared to the original one [Fig. 2(e)], and the RDD correlations acquire the form [67]:

$$C_{0j}(t) \propto (-1)^j \left(\mathcal{J}_{j-1}^2(2J_\parallel t) + 4 \sum_{k>0} k \mathcal{J}_{k+j-1}^2(2J_\parallel t) \right), \quad (2)$$

which corresponds to the staggered correlations of Fig. 2(d), which expand ballistically as for $\eta = 0$.

Effective SSH chain. Up to this point we have considered the hard-core model (1). Large but finite U may however play an important and surprising role in the defect dynamics. Up to second order in $J_{\perp,\parallel}/U$, the (again hard-core) model becomes $\hat{H}_{\text{eff}} = \hat{H}_0 + \Delta\hat{H}$, where

$$\Delta\hat{H} = -\frac{J_\perp^2}{U} \sum_j \hat{n}_{j,1}\hat{n}_{j,2} - \frac{J_\parallel^2}{U} \sum_{j,\alpha} \hat{n}_{j,\alpha}\hat{n}_{j+1,\alpha}$$

$$- \frac{J_\perp J_\parallel}{2U} \sum_{j,\alpha,\beta\neq\alpha} [\hat{b}_{j+1,\beta}^\dagger(\hat{n}_{j+1,\alpha} + \hat{n}_{j,\beta})\hat{b}_{j,\alpha} + \text{H.c.}]$$

$$- \frac{J_\parallel^2}{2U} \sum_{j,\alpha} (\hat{b}_{j+2,\alpha}^\dagger \hat{n}_{j+1,\alpha}\hat{b}_{j,\alpha} + \text{H.c.}), \quad (3)$$

with nearest-neighbor (NN) interactions along the legs and the rungs (first line), and collisionally-assisted hops along plaquette diagonals (second line), and between next-to-NN rungs (third line).

For $U = \infty$, leg hopping induces the same swap rate for $|\pm\rangle$ with $|2\rangle$ or $|0\rangle$. For finite U, the interplay of leg hopping and collisionally-induced diagonal hopping causes $|\pm\rangle$ to swap with $|2\rangle$ at a rate $J_\pm = J_\parallel(1 \pm 2J_\perp/U)$, while $|\pm\rangle$ and $|0\rangle$ still swap at rate $J_\parallel$ [Fig. 3(a)]. This is particularly relevant if, as typically in experiments, the initial DW presents isolated singlon defects. Consider a singlon defect at rung $j = 0$ in an otherwise perfect DW [Figs. 3(b) and 3(c)]. The defect experiences an effective staggered hopping described by the SSH Hamiltonian:

$$H_{\text{SSH}} = \frac{1}{2} \sum_j J_{j,j+1}(|\phi_j\rangle\langle\phi_{j+1}| + \text{H.c.}), \quad (4)$$

with $|\phi_j\rangle$ the state with the defect in rung j, and $J_{j,j+1} = J_1$ (J_2) for even (odd) j for $j \geq 0$, and the opposite for $j < 0$. The defect moves in an effective lattice of two SSH chains with opposite staggering that meet at the initial defect position [Figs. 3(b) and 3(c)]. Since one SSH chain is topological and the other is not, an exponentially localized zero-energy mode
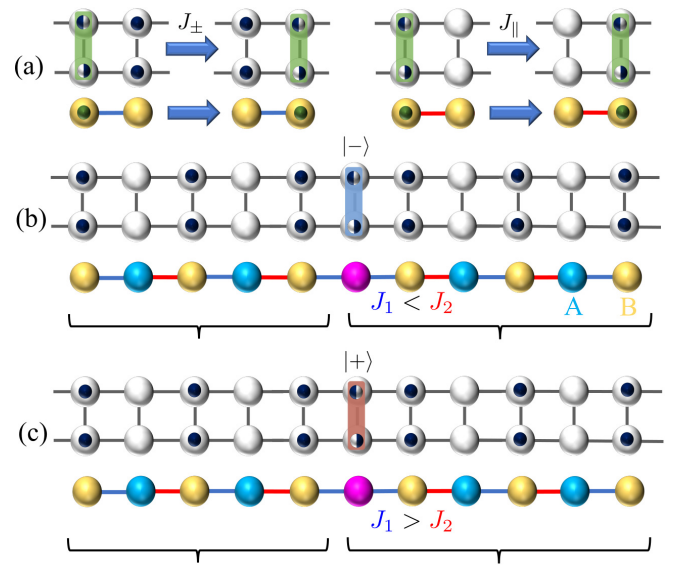

FIG. 3. (a) A singlon defect propagates by swapping its position with doubly occupied and empty rungs. Due to finite U, these swaps result in two different hopping rates (blue and red lines). The defect propagates in an effective lattice in which the right and the left of the initial defect position present opposite SSH staggering, illustrated for the case of a defect in what should have been an empty rung. (b) For a $|-\rangle$ defect (blue), $J_1 < J_2$, and the defect experiences topological localization. (c) For a $|+\rangle$ (brown), $J_1 > J_2$, and the defect displays nontopological localization. In the effective chain, light blue (yellow) sites indicate the A (B) sublattice.

appears at the interface [44,63–66]. We call the sublattice of even rungs, where the defect is initially, A, and the sublattice of odd rungs B.

Topological and nontopological localization. We consider first $J_1 < J_2$ [Fig. 3(b)]. This is the case in which a $|-\rangle$ ($|+\rangle$) defect occurs where $|0\rangle$ ($|2\rangle$) should have been, for which $J_1 = J_-$ ($J_\parallel$) and $J_2 = J_\parallel$ (J_+). At the interface between the SSH half-chains, the system presents a localized zero-energy edge mode [67], $|\psi\rangle = \sqrt{P_0} \sum_m e^{-|m|/2\xi} |\phi_{2m}\rangle$, with $\xi = \frac{1}{2\ln(J_2/J_1)}$, and $P_0 = |\langle\phi_0|\psi\rangle|^2 = (J_2^2 - J_1^2)/(J_2^2 + J_1^2)$. The defect (initially in $|\phi_0\rangle$) remains hence localized with probability P_0, and the localized population only occupies A rungs.

The situation changes radically if $J_1 > J_2$, which corresponds to a $|-\rangle$ ($|+\rangle$) defect where $|2\rangle$ ($|0\rangle$) should have been, for which $J_1 = J_\parallel$ (J_+) and $J_2 = J_-$ ($J_\parallel$). Topological localization is precluded because the zero-energy edge state has only support in the B sublattice [67]. However, localized states appear at the two ends of the spectrum [67], with opposite energies $\pm E$, with $E \simeq \frac{1}{2}[\sqrt{2}J_1 + \frac{J_2^2/4}{(\sqrt{2}-1)J_1}]$. The population of these localized states, results in partial localization of the defect, which oscillates with frequency $\Omega = E/\hbar$ between the A and B sublattices [67]. This may be intuitively understood from the case $J_2 \ll J_1$, for which the central A site and the symmetric superposition of the neighboring B sites form an isolated two-level system characterized by an oscillatory frequency $\Omega = \sqrt{2}J_1/2\hbar$.

Figure 4 shows the time evolution of the singlon defect probability $P_s(j)$ for $\eta = 16$ and $J_\perp/U = 0.5$ [73], for four

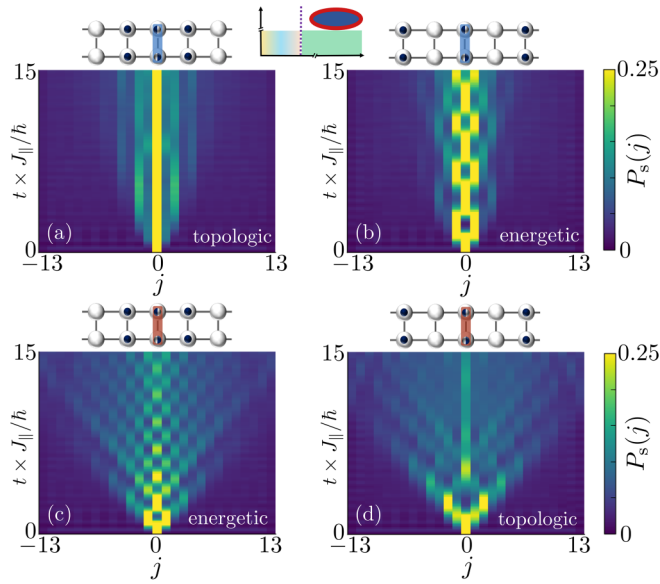FIG. 4. Time evolution of the probability of finding the defect in rung j, $P_s(j)$. The color bar saturates above 0.25. The initial defect position and state is indicated on top of each panel, with a blue (brown) box indicating a $|-\rangle$ ($|+\rangle$) defect. The inset in the top locates this figure in Fig. 1(c). MPS simulations of the full Bose-Hubbard Hamiltonian $\hat{H}$ with 27 sites, $\eta = 16$, $J_\perp/U = 1/2$, and bond dimension $\chi = 768$.

different cases: topological localization in Figs. 4(a) and 4(d), and nontopological localization in Figs. 4(b) and 4(c). Note the strikingly distinct dynamics in both cases, with clear oscillations between sublattice A and B in the nontopological case. Although the localization mechanism and the defect dynamics differ in the two regimes, the localized fraction is in any case very significant as long as J_1 and J_2 are sufficiently different. Hence, irrespective of the defect created and where it is produced, if $J_\perp/U$ is sufficiently large, we may expect strong localization of all singlon defects.

Other interaction-induced terms. The emergent SSH chain experienced by the defects demands the stability of the DW for finite U and $J_\parallel \ll J_\perp < U$. Projecting H_{eff} on the manifold of states without singlon defects [74], we obtain an effective model for doubly-occupied rungs [67], $\hat{H}_D = \frac{3J_\parallel^2}{2U} \sum_j (\hat{d}_j^\dagger \hat{d}_{j+1} + \hat{d}_{j+1}^\dagger \hat{d}_j - \frac{10}{3} \hat{n}_{d,j} \hat{n}_{d,j+1})$, with $\hat{d}_j$ the (hard-core boson) annihilation operator of doubly-occupied rungs, and $\hat{n}_{d,j} = \hat{d}_j^\dagger \hat{d}_j$. The hopping terms in $\hat{H}_D$ correspond to $|20\rangle \rightarrow |02\rangle$ swaps, which scramble the initial DW. Interestingly, the relatively strong NN interaction between doubly-occupied rungs makes the DW stable against those swaps [67]. Hence, quantum fluctuations of the DW order may lead for times $t > 2U/3J_\parallel^2$ to the blurring of the background, but they do not destroy the localization [67]. Furthermore, being hard-core bosons, singlon defects repel elastically [74]. NN interactions may lead to $|+, -\rangle \rightarrow |-, +\rangle$ swaps with a rate $J_\parallel^2/2U$, but these swaps are negligible for low defect densities [67]. Finally, collisionally assisted next-to-NN hopping is only relevant due to hops $|\pm, 2, 0\rangle \rightarrow |0, 2, \pm\rangle$, which scramble the DW. These processes occur with a rate $-J_\parallel^2/2U$, being neglible for $t < 2U/J_\parallel^2$.

Experimental realization. The emergent SSH chain experienced by each singlon defect is hence to a good approximation affected neither by the presence of neighboring defects, nor by quantum fluctuations of the DW or next-to-NN hops. Probing the regime $J_\parallel \ll J_\perp < U$ is readily accessible in on-going experiments [61]. Singlon-defect localization may be monitored in various ways. Current quantum gas microscopes [75] can deterministically create and measure $|+\rangle$ and $|-\rangle$ with single-rung resolution. The dynamics depicted in Fig. 4 can then be observed directly. Even without site-resolved state preparation, asymmetries in the defect creation between even and odd rungs can be used to access the localization dynamics. Under current experimental conditions [61] we expect that 80% of the created singlon defects are in even rungs, which should have been doubly occupied. One may hence monitor the imbalance $\mathcal{I} = 2\mathcal{N}_E - 1$, with $\mathcal{N}_E$ the number of singly-occupied even rungs. For $U = \infty$, defects propagate ballistically and $\mathcal{I}(t) = \mathcal{I}(0)\mathcal{J}_0(2J_\parallel t/\hbar)$. In contrast, topological and nontopological localization should result in a markedly different $\mathcal{I}(t)$, since topologically localized defects do not oscillate between sublattices, and nontopological defects oscillate between them with a frequency Ω.

Conclusions. Bose-Hubbard ladders initialized in a density wave provide an unexpected platform for the realization of an emergent interaction-enabled topological-nontopological interface of two SSH chains with opposite staggering, without the necessity of tailored external potentials. As a result, singlon defects experience two possible localization mechanisms, one topological and the other nontopological, characterized by strikingly distinct dynamics. This surprising link between topology and many-body quantum dynamics can be probed in ongoing experiments. In a broader context, our work illustrates how defect dynamics is determined by the background substrate they move through (here a density wave). This idea readily generalizes to different static backgrounds, e.g., a random background may result in localization without external disorder akin to disorder-free localization [76], and to dynamically coupled backgrounds, e.g., in bilayer settings defect motion reconfigures the initial state pattern and hence the effective tunneling rates. Our results also open further intriguing perspectives for the realization of emergent topological behavior in other platforms, in particular in synthetic ladders created using internal states [18,19,77].

---

[1] X.-G. Wen, *Colloquium:* Zoo of quantum-topological phases of matter, Rev. Mod. Phys. **89**, 041004 (2017).

[2] T. Senthil, Symmetry-protected topological phases of quantum matter, Annu. Rev. Condens. Matter Phys. **6**, 299 (2015).

[3] *The Quantum Hall Effect*, edited by R. E. Prange and S. M. Girvin (Springer, New York, NY, 1990)

[4] K. von Klitzing, T. Chakraborty, P. Kim, V. Madhavan, X. Dai, J. McIver, Y. Tokura, L. Savary, D. Smirnova, A. M. Rey, C. Felser, J. Gooth, and X. Qi, 40 years of the quantum Hall effect, Nat. Rev. Phys. **2**, 397 (2020).

[5] C.-Z. Chang, C.-X. Liu, and A. H. MacDonald, *Colloquium:* Quantum anomalous Hall effect, Rev. Mod. Phys. **95**, 011002 (2023).

[6] M. Z. Hasan and C. L. Kane, *Colloquium:* Topological insulators, Rev. Mod. Phys. **82**, 3045 (2010).

[7] X.-L. Qi and S.-C. Zhang, Topological insulators and superconductors, Rev. Mod. Phys. **83**, 1057 (2011).

[8] H. Luo, P. Yu, G. Li, and K. Yan, Topological quantum materials for energy conversion and storage, Nat. Rev. Phys. **4**, 611 (2022).

[9] M. J. Gilbert, Topological electronics, Commun. Phys. **4**, 70 (2021).

[10] O. Breunig and Y. Ando, Opportunities in topological insulator devices, Nat. Rev. Phys. **4**, 184 (2021).

[11] C. Nayak, S. H. Simon, A. Stern, M. Freedman, and S. Das Sarma, Non-Abelian anyons and topological quantum computation, Rev. Mod. Phys. **80**, 1083 (2008).

[12] J. Ningyuan, C. Owens, A. Sommer, D. Schuster, and J. Simon, Time- and site-resolved dynamics in a topological circuit, Phys. Rev. X **5**, 021031 (2015).

[13] M. Hafezi, S. Mittal, J. Fan, A. Migdall, and J. M. Taylor, Imaging topological edge states in silicon photonics, Nat. Photonics **7**, 1001 (2013).

[14] P. St-Jean, V. Goblot, E. Galopin, A. Lemaître, T. Ozawa, L. Le Gratiet, I. Sagnes, J. Bloch, and A. Amo, Lasing in topological edge states of a one-dimensional lattice, Nat. Photonics **11**, 651 (2017).

[15] R. Süsstrunk and S. D. Huber, Observation of phononic helical edge states in a mechanical topological insulator, Science **349**, 47 (2015).

[16] M. Atala, M. Aidelsburger, J. T. Barreiro, D. Abanin, T. Kitagawa, E. Demler, and I. Bloch, Direct measurement of the Zak phase in topological Bloch bands, Nat. Phys. **9**, 795 (2013).

[17] M. Atala, M. Aidelsburger, M. Lohse, J. T. Barreiro, B. Paredes, and I. Bloch, Observation of chiral currents with ultracold atoms in bosonic ladders, Nat. Phys. **10**, 588 (2014).

[18] B. K. Stuhl, H.-I. Lu, L. M. Aycock, D. Genkina, and I. B. Spielman, Visualizing edge states with an atomic Bose gas in the quantum Hall regime, Science **349**, 1514 (2015).

[19] M. Mancini, G. Pagano, G. Cappellini, L. Livi, M. Rider, J. Catani, C. Sias, P. Zoller, M. Inguscio, M. Dalmonte, and L. Fallani, Observation of chiral edge states with neutral fermions in synthetic Hall ribbons, Science **349**, 1510 (2015).

[20] G. Jotzu, M. Messer, R. Desbuquois, M. Lebrat, T. Uehlinger, D. Greif, and T. Esslinger, Experimental realization of the topological Haldane model with ultracold fermions, Nature (London) **515**, 237 (2014).

[21] M. Aidelsburger, M. Lohse, C. Schweizer, M. Atala, J. T. Barreiro, S. Nascimbène, N. R. Cooper, I. Bloch, and N. Goldman, Measuring the Chern number of Hofstadter bands with ultracold bosonic atoms, Nat. Phys. **11**, 162 (2015).

[22] M. Lohse, C. Schweizer, O. Zilberberg, M. Aidelsburger, and I. Bloch, A Thouless quantum pump with ultracold bosonic atoms in an optical superlattice, Nat. Phys. **12**, 350 (2016).

[23] S. Nakajima, T. Tomita, S. Taie, T. Ichinose, H. Ozawa, L. Wang, M. Troyer, and Y. Takahashi, Topological Thouless pumping of ultracold fermions, Nat. Phys. **12**, 296 (2016).

[24] M. Aidelsburger, S. Nascimbene, and N. Goldman, Artificial gauge fields in materials and engineered systems, C. R. Phys. **19**, 394 (2018).

[25] N. R. Cooper, J. Dalibard, and I. B. Spielman, Topological bands for ultracold atoms, Rev. Mod. Phys. **91**, 015005 (2019).

[26] A. W. W. Ludwig, Topological phases: classification of topological insulators and superconductors of non-interacting fermions, and beyond, Phys. Scr. **T168**, 014001 (2016).

[27] C.-K. Chiu, J. C. Y. Teo, A. P. Schnyder, and S. Ryu, Classification of topological quantum matter with symmetries, Rev. Mod. Phys. **88**, 035005 (2016).

[28] I. Bloch, J. Dalibard, and W. Zwerger, Many-body physics with ultracold gases, Rev. Mod. Phys. **80**, 885 (2008).

[29] I. Bloch, J. Dalibard, and S. Nascimbène, Quantum simulations with ultracold quantum gases, Nat. Phys. **8**, 267 (2012).

[30] C. Gross and I. Bloch, Quantum simulations with ultracold atoms in optical lattices, Science **357**, 995 (2017).

[31] F. Schäfer, T. Fukuhara, S. Sugawa, Y. Takasu, and Y. Takahashi, Tools for quantum simulation with ultracold atoms in optical lattices, Nat. Rev. Phys. **2**, 411 (2020).

[32] A. Browaeys and T. Lahaye, Many-body physics with individually controlled Rydberg atoms, Nat. Phys. **16**, 132 (2020).

[33] N. Goldman, J. C. Budich, and P. Zoller, Topological quantum matter with ultracold gases in optical lattices, Nat. Phys. **12**, 639 (2016).

[34] D.-W. Zhang, Y.-Q. Zhu, Y. X. Zhao, H. Yan, and S.-L. Zhu, Topological quantum matter with cold atoms, Adv. Phys. **67**, 253 (2018).

[35] W. S. Bakr, J. I. Gillen, A. Peng, S. Fölling, and M. Greiner, A quantum gas microscope for detecting single atoms in a Hubbard-regime optical lattice, Nature (London) **462**, 74 (2009).

[36] J. F. Sherson, C. Weitenberg, M. Endres, M. Cheneau, I. Bloch, and S. Kuhr, Single-atom-resolved fluorescence imaging of an atomic Mott insulator, Nature (London) **467**, 68 (2010).

[37] L. W. Cheuk, M. A. Nichols, M. Okan, T. Gersdorf, V. V. Ramasesh, W. S. Bakr, T. Lompe, and M. W. Zwierlein, Quantum-gas microscope for fermionic atoms, Phys. Rev. Lett. **114**, 193001 (2015).

[38] E. Haller, J. Hudson, A. Kelly, D. A. Cotta, B. Peaudecerf, G. D. Bruce, and S. Kuhr, Single-atom imaging of fermions in a quantum-gas microscope, Nat. Phys. **11**, 738 (2015).

[39] M. F. Parsons, F. Huber, A. Mazurenko, C. S. Chiu, W. Setiawan, K. Wooley-Brown, S. Blatt, and M. Greiner, Site-resolved imaging of fermionic ^{6}Li in an optical lattice, Phys. Rev. Lett. **114**, 213002 (2015).

[40] G. J. A. Edge, R. Anderson, D. Jervis, D. C. McKay, R. Day, S. Trotzky, and J. H. Thywissen, Imaging and addressing of individual fermionic atoms in an optical lattice, Phys. Rev. A **92**, 063406 (2015).

[41] M. Boll, T. A. Hilker, G. Salomon, A. Omran, J. Nespolo, L. Pollet, I. Bloch, and C. Gross, Spin- and density-resolved microscopy of antiferromagnetic correlations in Fermi-Hubbard chains, Science **353**, 1257 (2016).

[42] C. Gross and W. S. Bakr, Quantum gas microscopy for single atom and spin detection, Nat. Phys. **17**, 1316 (2021).

[43] C. Braun, R. Saint-Jalm, A. Hesse, J. Arceri, I. Bloch, and M. Aidelsburger, Real-space detection and manipulation of topological edge modes with ultracold atoms, Nat. Phys. **20**, 1306 (2024).

[44] W. P. Su, J. R. Schrieffer, and A. J. Heeger, Solitons in polyacetylene, Phys. Rev. Lett. **42**, 1698 (1979).

[45] S. de Léséleuc, V. Lienhard, P. Scholl, D. Barredo, S. Weber, N. Lang, H. P. Büchler, T. Lahaye, and A. Browaeys, Observation of a symmetry-protected topological phase of interacting bosons with Rydberg atoms, Science **365**, 775 (2019).

[46] J. Léonard, S. Kim, J. Kwan, P. Segura, F. Grusdt, C. Repellin, N. Goldman, and M. Greiner, Realization of a fractional quantum Hall state with ultracold atoms, Nature (London) **619**, 495 (2023).

[47] P. Lunt, P. Hill, J. Reiter, P. M. Preiss, M. Gałka, and S. Jochim, Realization of a Laughlin state of two rapidly rotating fermions, arXiv:2402.14814.

[48] F. D. M. Haldane, Nonlinear field theory of large-spin Heisenberg antiferromagnets: Semiclassically quantized solitons of the one-dimensional easy-axis Néel state, Phys. Rev. Lett. **50**, 1153 (1983).

[49] P. Sompet, S. Hirthe, D. Bourgund, T. Chalopin, J. Bibo, J. Koepsell, P. Bojović, R. Verresen, F. Pollmann, G. Salomon, C. Gross, T. A. Hilker, and I. Bloch, Realizing the symmetry-protected Haldane phase in Fermi–Hubbard ladders, Nature (London) **606**, 484 (2022).

[50] T. Langen, R. Geiger, and J. Schmiedmayer, Ultracold atoms out of equilibrium, Annu. Rev. Condens. Matter Phys. **6**, 201 (2015).

[51] A. P. Luca D'Alessio, Yariv Kafri and M. Rigol, From quantum chaos and eigenstate thermalization to statistical mechanics and thermodynamics, Adv. Phys. **65**, 239 (2016).

[52] E. Dagotto and T. M. Rice, Surprises on the way from one- to two-dimensional quantum magnets: The ladder materials, Science **271**, 618 (1996).

[53] E. Dagotto, Experiments on ladders reveal a complex interplay between a spin-gapped normal state and superconductivity, Rep. Prog. Phys. **62**, 1525 (1999).

[54] X. Li, E. Zhao, and W. Vincent Liu, Topological states in a ladder-like optical lattice containing ultracold atoms in higher orbital bands, Nat. Commun. **4**, 1523 (2013).

[55] R. Steinigeweg, F. Heidrich-Meisner, J. Gemmer, K. Michielsen, and H. De Raedt, Scaling of diffusion constants in the spin-$\frac{1}{2}$ xx ladder, Phys. Rev. B **90**, 094417 (2014).

[56] S.-S. Li, Z.-Y. Ge, and H. Fan, Localization of rung pairs in a hard-core Bose-Hubbard ladder, Phys. Rev. A **102**, 062409 (2020).

[57] D. Schubert, J. Richter, F. Jin, K. Michielsen, H. De Raedt, and R. Steinigeweg, Quantum versus classical dynamics in spin models: Chains, ladders, and square lattices, Phys. Rev. B **104**, 054415 (2021).

[58] T. Rakovszky, C. W. von Keyserlingk, and F. Pollmann, Dissipation-assisted operator evolution method for capturing hydrodynamic transport, Phys. Rev. B **105**, 075131 (2022).

[59] G. A. Domínguez-Castro, T. Bilitewski, D. Wellnitz, A. M. Rey, and L. Santos, Relaxation in dipolar spin ladders: From pair production to false-vacuum decay, Phys. Rev. A **110**, L021302 (2024).

[60] S. Hirthe, T. Chalopin, D. Bourgund, P. Bojović, A. Bohrdt, E. Demler, F. Grusdt, I. Bloch, and T. A. Hilker, Magnetically mediated hole pairing in fermionic ladders of ultracold atoms, Nature (London) **613**, 463 (2023).

[61] J. F. Wienand, S. Karch, A. Impertro, C. Schweizer, E. McCulloch, R. Vasseur, S. Gopalakrishnan, M. Aidelsburger, and I. Bloch, Emergence of fluctuating hydrodynamics in chaotic quantum systems, Nat. Phys. **20**, 1732 (2024).

[62] M. Leder, C. Grossert, L. Sitta, M. Genske, A. Rosch, and M. Weitz, Real-space imaging of a topologically protected edge state with ultracold atoms in an amplitude-chirped optical lattice, Nat. Commun. **7**, 13112 (2016).

[63] C. Poli, M. Bellec, U. Kuhl, F. Mortessagne, and H. Schomerus, Selective enhancement of topologically induced interface states in a dielectric resonator chain, Nat. Commun. **6**, 6710 (2015).

[64] E. J. Meier, F. A. An, and B. Gadway, Observation of the topological soliton state in the Su–Schrieffer–Heeger model, Nat. Commun. **7**, 13986 (2016).

[65] W. Cai, J. Han, F. Mei, Y. Xu, Y. Ma, X. Li, H. Wang, Y. P. Song, Z.-Y. Xue, Z.-q. Yin, S. Jia, and L. Sun, Observation of topological magnon insulator states in a superconducting circuit, Phys. Rev. Lett. **123**, 080501 (2019).

[66] S. Lin, L. Zhang, T. Tian, C.-K. Duan, and J. Du, Dynamic observation of topological soliton states in a programmable nanomechanical lattice, Nano Lett. **21**, 1025 (2021).

[67] See Supplemental Material at http://link.aps.org/supplemental/10.1103/PhysRevResearch.7.L012012 for a detailed discussion on the stability analysis of the DW in the hard-core regime, the defect theory explaining the staggered RRD correlations for $\eta > 2$, the topological edge modes, the non-topologically localized states, the stability of the DW against swaps $20 \to 02$, extended numerical results for lower η values, details on the MPS calculations, and defect-defect interactions including Refs. [68–72].

[68] T. Bilitewski and A. M. Rey, Manipulating growth and propagation of correlations in dipolar multilayers: From pair production to bosonic Kitaev models, Phys. Rev. Lett. **131**, 053001 (2023).

[69] G. Vidal, Efficient simulation of one-dimensional quantum many-body systems, Phys. Rev. Lett. **93**, 040502 (2004).

[70] A. T. Sornborger and E. D. Stewart, Higher-order methods for simulations on quantum computers, Phys. Rev. A **60**, 1956 (1999).

[71] J. Bezanson, A. Edelman, S. Karpinski, and V. B. Shah, Julia: A fresh approach to numerical computing, SIAM Rev. **59**, 65 (2017).

[72] M. Fishman, S. R. White, and E. M. Stoudenmire, The ITensor Software Library for Tensor Network Calculations, SciPost Phys. Codebases, 4 (2022).

[73] Note that $J_\perp/U = 1/2$ lies clearly beyond the validity regime of perturbation theory, explaining why the localization in Fig. 4(a) does not have zero localization length, as may have been expected from $J_- = J_\parallel(1 - 2J_\perp/U) = 0$. However, the qualitative features of topological and non-topological localization remain valid.

[74] Similar to defect creation $|2, 0\rangle \leftrightarrow |\pm, \pm\rangle$ is non-resonant due to the rung energy, and $|2, 0\rangle \leftrightarrow |\pm, \mp\rangle$, which would be resonant, cannot be induced by leg hopping due to leg exchange symmetry.

[75] A. Impertro, S. Karch, J. F. Wienand, S. J. Huh, C. Schweizer, I. Bloch, and M. Aidelsburger, Local readout and control of current and kinetic energy operators in optical lattices, Phys. Rev. Lett. **133**, 063401 (2024).

[76] A. Smith, J. Knolle, D. L. Kovrizhin, and R. Moessner, Disorder-free localization, Phys. Rev. Lett. **118**, 266601 (2017).

[77] S. Kolkowitz, S. L. Bromley, T. Bothwell, M. L. Wall, G. E. Marti, A. P. Koller, X. Zhang, A. M. Rey, and J. Ye, Spin–orbit-coupled fermions in an optical lattice clock, Nature (London) **542**, 66 (2017).